

Head-to-Head Domain Wall Structures in Wide Permalloy Strips

Virginia Estévez* and Lasse Laurson

*COMP Centre of Excellence and Helsinki Institute of Physics,
Department of Applied Physics, Aalto University,
P.O.Box 11100, FI-00076 Aalto, Espoo, Finland.*

We analyze the equilibrium micromagnetic domain wall structures encountered in Permalloy strips of a wide range of thicknesses and widths, with strip widths up to several micrometers. By performing an extensive set of micromagnetic simulations, we show that the equilibrium phase diagram of the domain wall structures exhibits in addition to the previously found structures (symmetric and asymmetric transverse walls, vortex wall) also double vortex and triple vortex domain walls for large enough strip widths and thicknesses. Also several metastable domain wall structures are found for wide and/or thick strips. We discuss the details of the relaxation process from random magnetization initial states towards the stable domain wall structure, and show that our results are robust with respect to changes of e.g. the magnitude of the Gilbert damping constant and details of the initial conditions.

PACS numbers: 75.60.Ch, 75.78.Cd

I. INTRODUCTION

During the last decade, a lot of effort has been devoted to understand static and dynamic properties of magnetic domain walls (DWs) in ferromagnetic nanostructures such as nanowires and -strips. These studies have been largely driven by promising technological applications based on domain walls and their dynamics, in particular memory^{1,2} and logic devices³⁻⁵. In typical experiments DWs are driven by either applied magnetic fields^{6,7} or spin-polarized electric currents⁸⁻¹¹. The resulting DW dynamics depends crucially on the micromagnetic DW structure, typically involving various internal degrees of freedom. These are essential e.g. for the emergence of the Walker breakdown¹², an instability occurring when the DW internal degrees of freedom get excited by a strong external drive (a magnetic field H or a spin-polarized current J exceeding the Walker field H_W or current J_W , respectively), limiting the propagation velocity of the DWs.

Two main classes of ferromagnetic materials have been extensively studied within the strip geometry. Materials with a high perpendicular magnetic anisotropy (PMA¹³⁻¹⁶) exhibit simple and narrow DWs of the Bloch and/or Néel type. For $H > H_W$ or $J > J_W$, repeated transitions between these two structures are observed¹⁶. The second class of systems includes soft (low anisotropy) magnetic materials^{13,14} such as Permalloy, where in-plane domain magnetization along the long axis of the strip is induced by shape anisotropy. By using various experimental techniques^{17,18} and micromagnetic simulations, it has been established that the equilibrium DW structures separating these in-plane domains are more complex, and depend crucially on the sample geometry¹⁹⁻²². Transverse DWs (TWs) and asymmetric transverse DWs (ATWs) are observed for narrow and thin strips²²⁻²⁷, while in wider and thicker strips one encounters the vortex DW (VW)^{22,24-26,28,29}. In addition, various metastable DW structures with higher en-

ergy may be found^{18,28-31}. For $H > H_W$ or $J > J_W$, the DW structures exhibit dynamical evolution: for TWs, repeated nucleation and propagation of an antivortex across the strip width takes place¹⁹. Similarly, in VWs the vortex core performs oscillatory back and forth perpendicular motion¹⁹.

In Permalloy strips with even larger widths and/or thicknesses, one might expect also other, possibly more complicated equilibrium DW structures. For wider strips shape anisotropy is less important, implying that energy minima with more complex spin structures closing the flux more efficiently than TWs, ATWs or VWs may appear. Indeed, e.g. double and triple vortex DWs have been observed in experiments on wide strips²⁸, but they have been attributed to current-induced vortex nucleation resulting in metastable DW structures. Consequently, a pertinent and fundamental question is what are the possible intermediate equilibrium DW structures observable when the lateral Permalloy strip dimensions increase from those corresponding to the typical nanostrip geometry (with TW, ATW or VW as the stable DW structure) to strip widths of micrometers and beyond.

In this paper we present an extensive numerical study of the equilibrium and metastable micromagnetic DW structures in Permalloy strips, with the strip widths up to an order of magnitude larger than before¹⁹⁻²⁴. Contrary to previous studies focusing on comparing the energies of different *a priori* known DW structures¹⁹⁻²⁴, we perform micromagnetic simulations of relaxation dynamics from random initial states towards the stable DW structures. In addition to the previously observed TW, ATW and VW DWs, we find also DWs with equilibrium double and triple vortex structures for wide and/or thick enough strips. The last structure is encountered only in the very largest system sizes we were able to simulate. Moreover, for wide strips we find a rich variety of metastable DWs with even more complex micromagnetic structures. We demonstrate that our results are robust with respect to changes of the magnitude of the Gilbert damping con-

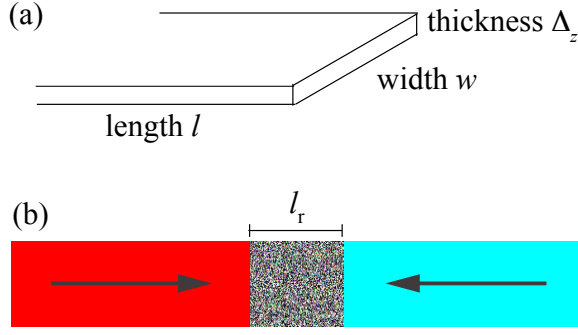


FIG. 1. (color online) (a) Geometry of the Permalloy strip. (b) A top view of the magnetization in the initial state. Magnetization points along the long axis of the strip within the two domains (as indicated by the arrows) forming a head-to-head configuration. In between them, a region of random magnetization (of length l_r) has been included.

stant or using different initial conditions for the relaxation process. Our results underline the crucial role of topological defects for physics of DWs in soft strips, and that of micromagnetic simulations for finding the true equilibrium DW structure.

II. MICROMAGNETIC SIMULATIONS

The system studied is a Permalloy strip of width w and thickness Δ_z , satisfying $\Delta_z \ll w$, see Fig. 1 (a). In the micromagnetic simulations, magnetic charges are compensated on the left and right ends of the strip, to mimic an infinitely long strip; the actual simulated length satisfies $l \geq 4w$ for all cases considered. The initial state from which the relaxation towards a stable DW structure starts is an in-plane head-to-head domain structure, with a region of random magnetization of length l_r in the middle of the sample, see Fig. 1 (b). If not specified otherwise, we consider $l_r = 2w$. Material parameters of Permalloy are used, i.e. saturation magnetization $M_s = 860 \times 10^3$ A/m and exchange constant $A_{\text{ex}} = 13 \times 10^{-12}$ J/m. The typical Gilbert damping constant for Permalloy is $\alpha = 0.01$, but here we analyze also the influence of α on the relaxation process, and thus consider also other values. For simplicity, we set the temperature T to zero, and focus on the ideal case of strips free of any structural disorder or impurities.

The simulations are performed using the GPU-accelerated micromagnetic code MuMax3^{32–34}, offering a significant speedup as compared to CPU codes for the large system sizes we consider here. To calculate the magnetization dynamics of the system, the Landau-Lifshitz-Gilbert equation^{35,36},

$$\partial \mathbf{m} / \partial t = \gamma \mathbf{H}_{\text{eff}} \times \mathbf{m} + \alpha \mathbf{m} \times \partial \mathbf{m} / \partial t, \quad (1)$$

is solved numerically. Here, \mathbf{m} is the magnetization, γ the gyromagnetic ratio, and \mathbf{H}_{eff} the effective field, with

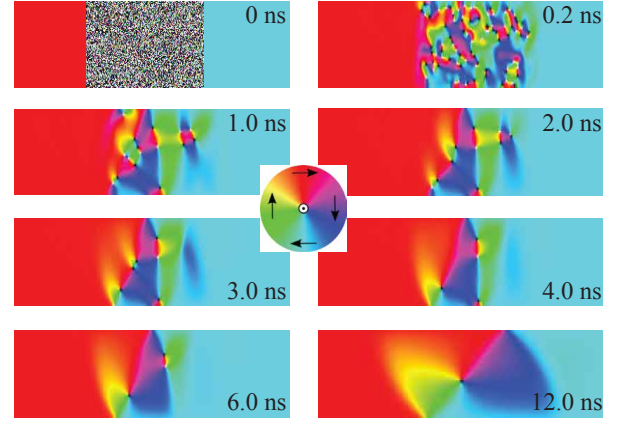


FIG. 2. (color online) An example of the temporal evolution of the relaxation, with $w = 420$ nm, $\Delta_z = 10$ nm, $\alpha = 3$ and $l_r = 2w$. Relaxation towards the equilibrium DW structure (here, a VW) takes place via coarsening dynamics of the defect structure in the magnetic texture. The colorwheel in the middle shows the mapping between magnetization directions and colors.

contributions due to exchange, Zeeman, and demagnetizing energies. The size of the discretization cell used depends on the system size, but is always bounded by the exchange length, $\Lambda = (2A/\mu_0 M_s^2)^{1/2} \approx 5$ nm, in the in-plane directions, and equals Δ_z in the out-of-plane direction.

III. RESULTS

We start by considering the effect of varying α and l_r on the relaxation process. Fig. 2 shows an example of the time evolution of $\mathbf{m}(\mathbf{r}, t)$ for $w = 420$ nm, $\Delta_z = 10$ nm, $\alpha = 3$ and $l_r = 2w$. The initially random magnetization evolves via coarsening of the defect structure of the magnetization texture towards the stable DW (here, a VW). During the relaxation, the total energy E of the system decreases in a manner that for a given geometry (w and Δ_z) depends on both α and l_r , see Fig. 3 (a) and (b) where $w = 5120$ nm and $\Delta_z = 20$ nm, is considered. For instance, E decreases faster for an intermediate α [Fig. 3 (a)]. We attribute this behavior to the balance between inertial effects related to precession favored by a small α , helping to overcome energy barriers, and the higher rate of energy dissipation due to a large α . Thus, the relaxation time to reach a (meta)stable DW structure depends on α . Fig. 3 (b) illustrates that for a fixed α , systems with a larger l_r relax more slowly. Fig. 3 (c) shows that on average, the early-time relaxation of E towards its final value E_f exhibits temporal power-law decay, $\langle E - E_f \rangle \propto t^{-\beta}$ with $\beta \approx 1.3$ for the $\alpha = 0.3$ case shown, possibly related to collective effects due to interactions between several topological defects during early stages of relaxation (Fig. 2).

In general, the final (meta)stable DW structure may

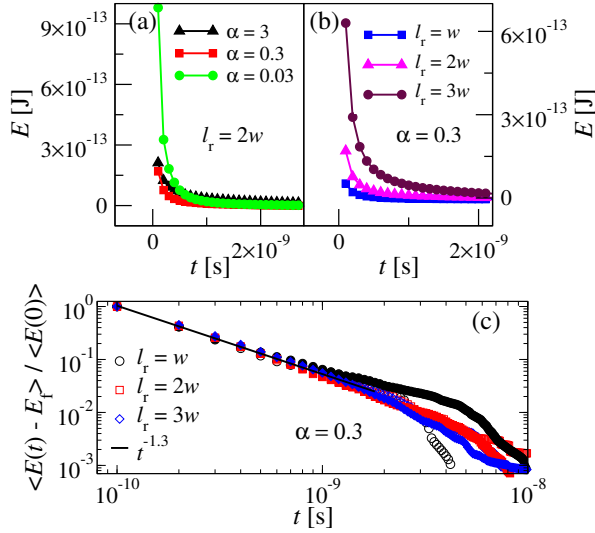


FIG. 3. (color online) The energy $E(t)$ as a function of time t for $w = 5120$ nm and $\Delta_z = 20$ nm. (a) For different values of α and $l_r = 2w$. (b) For different values of l_r , and $\alpha = 0.3$ [resulting in the fastest relaxation in (a)]. (c) shows that on average, the early time decay of $E(t)$ towards its final value E_f obeys $\langle E(t) - E_f \rangle \propto t^{-\beta}$. For the $\alpha = 0.3$ case shown here, $\beta \approx 1.3$. Empty (filled) symbols in (c) correspond to $w = 420$, $\Delta_z = 10$ nm ($w = 860$, $\Delta_z = 20$ nm).

depend on the realization of the random initial state. Thus, we consider 21 realizations of the initial random magnetization for each w and Δ_z , and compare the energies of the resulting relaxed configurations. The structure with the lowest energy is chosen as the equilibrium structure, while others with higher energy are metastable states. Although, as discussed above, the relaxation times depend on α and l_r , the equilibrium DW structure is found to be independent of α and l_r in the range considered, i.e. $\alpha \in [0.01, 3]$ and $l_r \in [w, 3w]$. Thus, in what follows, we will use $\alpha = 3$ and $l_r = 2w$.

The main results of this paper are summarized in Figs. 4 and 5, showing the phase diagram of the equilibrium DW structures for w ranging from 120 to 5120 nm, and Δ_z from 5 to 25 nm, and examples of these structures, respectively. For small w , we recover the previous results^{19–22}, i.e. phases corresponding to TW, ATW and VW, shown in Fig. 5 (a), (b) and (c), respectively.

For larger strip widths (w approaching or exceeding $1\mu\text{m}$, depending on Δ_z , see Fig. 4), a new equilibrium micromagnetic DW structure, a double vortex wall (DVW), is observed. This structure consists of two vortices with opposite sense of rotation of the magnetization around the vortex core, see Fig. 5 (d). At the phase boundary (blue triangle symbols pointing left in Fig. 4), VW and DVW have the same energy. The DVW phase spans a relatively large area within the (w, Δ_z) space, highlighting the robustness of our results.

In addition, a second new phase, with a triple-vortex wall (TVW) as the equilibrium structure [see Fig. 5 (e)],

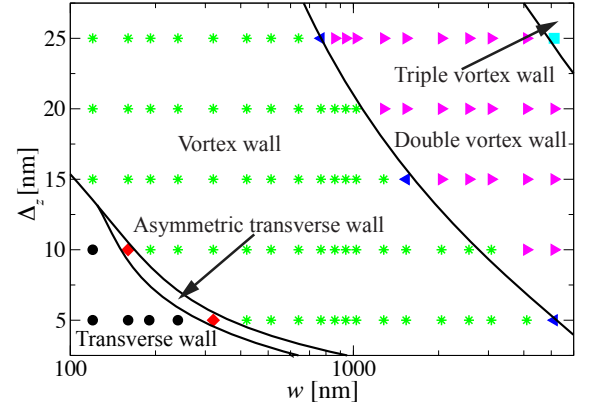


FIG. 4. (color online) Phase diagram of the equilibrium DW structure in Permalloy strips of various thicknesses (from $\Delta_z = 5$ to 25 nm) and widths ranging from $w = 120$ nm up to 5120 nm. The symbols correspond to observations of the various equilibrium DW structures, with phase boundaries shown as solid lines. Examples of the DW structures corresponding to the 5 different phases are shown in Fig. 5.

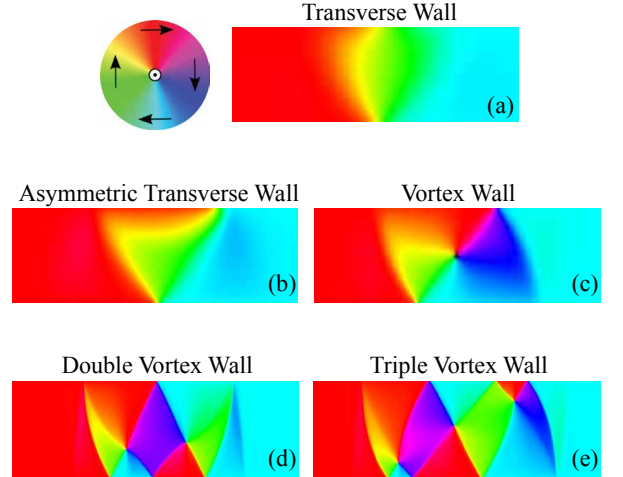


FIG. 5. (color online) Examples of the different equilibrium micromagnetic DW structures: (a) TW for $w = 120$ nm and $\Delta_z = 5$ nm, (b) ATW for $w = 160$ nm and $\Delta_z = 10$ nm, (c) VW for $w = 640$ nm and $\Delta_z = 15$ nm, (d) DVW for $w = 2560$ nm and $\Delta_z = 20$ nm, and (e) TVW for $w = 5120$ nm and $\Delta_z = 25$ nm. The colorwheel (top left) shows the mapping between magnetization directions and colors.

is found for the very largest system sizes we have been able to simulate. The middle vortex of the TVW has an opposite sense of rotation to the other two. For $w = 5120$ nm and $\Delta_z = 25$ nm, DVW and TVW have the same energy (the cyan square symbol in the top right corner of Fig. 4), suggesting the presence of a phase boundary between the two structures. Indeed, by performing a set of 10 additional simulations with $w = 6144$ nm and $\Delta_z = 25$ nm (i.e. outside the phase diagram in Fig. 4), suggests that TVW is the equilibrium DW structure for very large strip widths. This structure has been observed in experiments

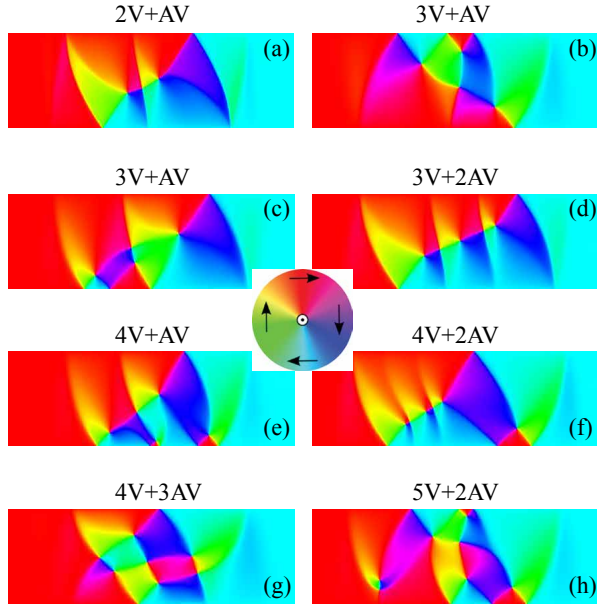


FIG. 6. (color online) Examples of metastable DW structures observed for a system with $w = 5120$ nm and different thicknesses Δ_z : (a) Two vortices and an antivortex (2V+AV), $\Delta_z = 25$ nm, (b) and (c) three vortices and an antivortex (3V+AV), $\Delta_z = 5$ nm, (d) three vortices and two antivortices (3V+2AV), $\Delta_z = 10$ nm, (e) four vortices and an antivortex (4V+AV), $\Delta_z = 5$ nm, (g) four vortices and three antivortices (4V+3AV), $\Delta_z = 5$ nm, and (h) five vortices and two antivortices (5V+2AV), $\Delta_z = 5$ nm.

as a metastable state for smaller systems^{28,29}. Notice also that the middle part of the TVW [Fig. 5 (e)], exhibiting four line-like 90° DWs meeting at a vortex core in the middle of the TVW, resembles the typical Landau flux-closure magnetization patterns observed for rectangular Permalloy thin films^{37–39}.

Following the relaxation from a random magnetization initial state, the system may in general end up into various metastable states with higher energy than that of the equilibrium DW. Sometimes these metastable states have even a higher probability than the equilibrium one, estimated here from the sample of 21 relaxed configurations. Fig. 6 shows some of the metastable states found for a large strip with $w = 5120$ nm and different values of Δ_z ; for strips with smaller lateral dimensions, different metastable states tend to be less numerous and have a simpler structure. Despite their apparent complexity, all the metastable DW structures shown in Fig. 6 respect the basic principles of topology of DWs. Each of the DWs are composed of topological defects, with an associated winding number: +1 for vortices, -1 for antivortices, and $\pm 1/2$ for edge defects⁴⁰. In a DW all the topological defects have to be compensated, i.e. the total winding number is equal to zero. In the case of the DVW, the two topological vortex defects are compensated by four edge defects [Fig. 5 (d)]. For the metastable state of two

vortices (with the same sense of rotation) and an antivortex [2V+AV, see Fig. 6 (a)], there are two vortices and only two edge defects. Thus, in order to compensate the topological defects, also an antivortex appears. In general, we have observed that in a DW with N vortices with the same sense of rotation, there must be $N - 1$ antivortices to get a zero total winding number, see Fig. 6 (a) and (d) for examples with 2V+AV and 3V+2AV configurations, respectively. When some of the vortices have opposite sense of rotation, more complex scenarios are encountered, with examples shown in Figs. 6 (b), (c), (e), (f), (g) and (h). Notice also that two DW structures with the same elements can look very different, see e.g. the two 3V+AV DWs shown in Figs. 6 (b) and (c). All the DW structures found, both the equilibrium ones in Fig. 5 and the metastable states in Fig. 6 obey the principle of compensation of topological defects to yield a total winding number of zero. The richness of the equilibrium phase diagram and the large collection of metastable states indicate that for wide/thick strips in particular, the micromagnetic energy landscape is quite complex, with a large number of local minima. This is also in agreement with our observations of power-law energy relaxation.

IV. SUMMARY AND CONCLUSIONS

To summarize, we have performed an extensive set of micromagnetic simulations to study the equilibrium and metastable DW structures in Permalloy strips of a wide range of widths and thicknesses, as well as the relaxation dynamics starting from random magnetization initial states. The general trend of our results is that both the equilibrium and metastable DW configurations become increasingly complex (i.e. they consist of an increasing number of topological defects) as the lateral strip dimensions increase. We note that somewhat analogous behaviour - i.e. existence of equilibrium magnetization configurations with increasing complexity as the system size increases - is observed also in some other systems such as three-dimensional cylindrical elements with perpendicular anisotropy^{41,42}.

Several remarks are in order: first, for strips with even larger lateral dimensions one may in principle expect more complex DW patterns - possibly with four or more vortices with alternating sense of rotation. These, however, are currently beyond the reach of our available computing resources. Second, our phase diagram allows one to check if experimental observations of the various DW structures in wider strips are equilibrium configurations or metastable states. According to our review of the experimental literature, most observations of DVWs and TVWs appear to be metastable states^{28,29}. Third, while the equilibrium structures we find are certainly stable in the absence of external perturbations such as applied magnetic fields, it remains to be seen how their field driven dynamics is like, and whether wide strips with a relatively weak shape anisotropy are able to support the

DWs as compact objects also when external perturbations are being applied⁴³.

ACKNOWLEDGMENTS

We thank Mikko J. Alava for a critical reading of the manuscript. This work has been supported by the Academy of Finland through its Centres of Excellence Programme (2012-2017) under project no. 251748, and an Academy Research Fellowship (LL, project no. 268302). We acknowledge the computational resources provided by the Aalto University School of Science “Science-IT” project, as well as those provided by CSC (Finland).

-
- * virginia.esteveznuno@aalto.fi
- ¹ S. S. P. Parkin, M. Hayashi and L. Thomas, *Science* **320**, 190 (2008).
 - ² S. E. Barnes, J. Ieda and S. Maekawa, *Appl. Phys. Lett.* **89**, 122507 (2006).
 - ³ R. P. Cowburn and M. E. Welland, *Science* **287**, 1466 (2000).
 - ⁴ D. A. Allwood, G. Xiong, M. D. Cooke, C. C. Faulkner, D. Atkinson, N. Vernier and R. P. Cowburn, *Science* **296**, 2003 (2002).
 - ⁵ D. A. Allwood, G. Xiong, C. C. Faulkner, D. Atkinson, D. Petit and R. P. Cowburn, *Science* **309**, 1688 (2005).
 - ⁶ T. Ono, H. Miyajima, K. Shigeto, K. Mibu, N. Hosoiito and T. Shinjo, *Science* **284**, 468 (1999).
 - ⁷ G. S. D. Beach, C. Nistor, C. Knutson, M. Tsoi and J. L. Erskine, *Nature Mater.* **4**, 741 (2005).
 - ⁸ M. Kläui, C. A. F. Vaz, J. A. C. Bland, W. Wernsdorfer, G. Faini, E. Cambril and L. J. Heyderman, *Appl. Phys. Lett.* **83**, 105 (2003).
 - ⁹ A. Thiaville, Y. Nakatani, J. Miltat and N. Vernier, *J. Appl. Phys.* **95**, 7049 (2004).
 - ¹⁰ M. Kläui, P.-O. Jubert, R. Allenspach, A. Bischof, J. A. C. Bland, G. Faini, U. Rüdiger, C. A. F. Vaz, L. Vila and C. Vauille, *Phys. Rev. Lett.* **95**, 026601 (2005).
 - ¹¹ N. Vernier, D. A. Allwood, D. Atkinson, M. D. Cooke and R. P. Cowburn, *EPL* **65**, 526 (2004).
 - ¹² N. L. Schryer and L. R. Walker, *Journal of Applied Physics* **45**, 5406 (1974).
 - ¹³ K.H.J. Buschow and F.R. de Boer, *Physics of Magnetism and Magnetic Materials*. Kluwer Academic Publishers (2003).
 - ¹⁴ J.M.D. Coey, *Magnetism and Magnetic Materials*, Cambridge University Press.
 - ¹⁵ O. Boulle, J. Kimling, P. Warnicke, M. Kläui, U. R. Rüdiger, G. Malinowski, H. J. M. Swagten, B. Koopmans, C. Ulysse and G. Faini, *Phys. Rev. Lett.* **101**, 216601 (2008).
 - ¹⁶ E. Martinez, *J. Phys.: Condens. Matter* **24** (2012) 024206.
 - ¹⁷ H. Kronmüller and S. S. P. Parkin (eds), *Handbook of Magnetism and Advanced Materials* **3** (Chichester, Wiley, 2007).
 - ¹⁸ M. Kläui, *J. Phys.: Condens. Matter* **20**, 313001 (2008).
 - ¹⁹ A. Thiaville and Y. Nakatani, in *Spin Dynamics in Confined magnetic Structures III*, edited by B. Hillebrands and A. Thiaville, *Topics in Applied Physics* **101** (Springer, Berlin, 2006).
 - ²⁰ R. D. McMichael and M. J. Donahue, *IEEE Trans. Magn.* **33**, 4167 (1997).
 - ²¹ Y. Nakatani, A. Thiaville and J. Miltat, *J. Magn. Magn. Mater.* **290-291**, 750 (2005).
 - ²² M. Kläui, C. A. F. Vaz, J. A. C. Bland, L. J. Heyderman, F. Nolting, A. Pavlovskaya, E. Bauer, S. Cherifi, S. Heun, and A. Locatelli, *Appl. Phys. Lett.* **85**, 5637 (2004).
 - ²³ S. Jamet, N. Rougemaille, J. C. Toussaint, and O. Fruchart, *arXiv preprint arXiv:1412.0679* (2014).
 - ²⁴ Y. Nozaki, K. Matsuyama, T. Ono, and H. Miyajima, *Jpn. J. Appl. Phys. Vol. 38* (1999) 6282.
 - ²⁵ M. Kläui, C. A. F. Vaz, J. A. C. Bland, T. L. Monchesky, J. Unguris, E. Bauer, S. Cherifi, S. Heun, A. Locatelli, L. J. Heyderman, and Z. Cui, *Phys. Rev. B* **68**, 134426 (2003).
 - ²⁶ M. Kläui, U. Rüdiger, C. A. F. Vaz, J. A. C. Bland, S. Cherifi, A. Locatelli, S. Heun, A. Pavlovskaya, E. Bauer, and L. J. Heyderman, *Appl. Phys. Lett.* **99**, 08G308 (2006).
 - ²⁷ D. Backes, C. Schieback, M. Kläui, F. Junginger, H. Ehrke, P. Nielaba, U. Rüdiger, L. J. Heyderman, C. S. Chen, T. Kasama, R. E. Dunin-Borkowski, C. A. F. Vaz, and J. A. C. Bland, *Appl. Phys. Lett.* **91**, 112502 (2007).
 - ²⁸ M. Kläui, M. Laufenberg, L. Heyne, D. Backes, U. Rüdiger, C. A. F. Vaz, J. A. C. Bland, L. J. Heyderman, S. Cherifi, A. Locatelli, T. O. Montes, and L. Aballe, *Appl. Phys. Lett.* **88**, 232507 (2006).
 - ²⁹ E.-M. Hempe, M. Kläui, T. Kasama, D. Backes, F. Junginger, S. Krzyk, L. J. Heyderman, R. Dunin-Borkowski, and U. Rüdiger, *phys. stat. sol.(a)* **204**, 3922 (2007).
 - ³⁰ C. A. F. Vaz, M. Kläui, L. J. Heyderman, C. David, F. Nolting, and J. A. C. Bland, *Phys. Rev. B* **72**, 224426 (2005).
 - ³¹ M.H. Park, Y.K. Hong, B.C. Choi, M. J. Donahue, H.Han, and S.H. Gee, *Phys. Rev. B* **73**, 094424 (2006).
 - ³² <http://mumax.github.io>
 - ³³ A. Vansteenkiste and B. Van de Wiele, *J. Magn. Magn. Mater.* **323**, 2585 (2011).
 - ³⁴ A. Vansteenkiste *et al.*, *AIP Advances* **4**, 107133 (2014).
 - ³⁵ T. L. Gilbert, *IEEE Trans. Magn.* **40**, 3443 (2004).
 - ³⁶ W. F. Brown, Jr., *Micromagnetics*. (New York, Wiley, 1963).
 - ³⁷ T. Shinjo, T. Okuno, R. Hassdorf, K. Shigeto, and T. Ono, *Science* **289**, 930 (2000).
 - ³⁸ A Wachowiak, J. Wiebe, M. Bode, O. Pietzsch, M. Morgenstern, and R. Wiesendanger, *Science* **298**, 577 (2002).
 - ³⁹ P. Fischer, M.-Y. Im, S. Kasai, K. Yamada, T. Ono, and A. Thiaville, *Phys. Rev. B* **83**, 212402 (2011).
 - ⁴⁰ O. Tchernyshyov and G.-W. Chern, *Phys. Rev. Lett.*, **95**, 197204 (2005).

- ⁴¹ C. Moutafis, S. Komineas, C. A. F. Vaz, J. A. C. Bland, T. Shima, T. Seki, and K. Takanashi, Phys. Rev. B **76**, 104426 (2007).
- ⁴² N. Vukadinovic and F. Boust, Phys. Rev. B **78**, 184411 (2008).
- ⁴³ C. Zinoni, A. Vanhaverbeke, P. Eib, G. Salis, and R. Allenspach, Phys. Rev. Lett. **107**, 207204 (2011).